SUPPLEMENTARY INFORMATION

for

Molecular-level degradation pathways of black phosphorus revealed by mass spectrometry fingerprinting

Xiu Huang,[a,b] Yong Li,[a] Guangbo Qu,[a] Xue-Feng Yu,[c] Dong Cao,[a] Qian Liu,*[a,d,e] Guibin Jiang[a,e]

[a] *State Key Laboratory of Environmental Chemistry and Ecotoxicology, Research Center for Eco-Environmental Sciences, Chinese Academy of Sciences, Beijing 100085, China*

[b] *West China School of Public Health and West China Fourth Hospital, Sichuan University, Sichuan 610065, China*

[c] *Materials Interfaces Center, Shenzhen Institutes of Advanced Technology, Chinese Academy of Sciences, Shenzhen 518055, China*

[d] *Institute of Environment and Health, Jianghan University, Wuhan 430056, China*

[e] *College of Resources and Environment, University of Chinese Academy of Sciences, Beijing 100190, China*

Email: qianliu@rcees.ac.cn

Contents

1. Supplementary Tables
2. Supplementary Figures

1. Supplementary Tables

Table S1. Analytical figures of merit of BP materials by dual-ion-mode LDI-TOF MS.

Material	Ion mode	m/z[a]	LOD (pg/mL)[b]	Shot-to-shot RSD (n = 20)[c]	Sample-to-sample RSD (n = 15)[d]	Linear range (μg/mL)	Calibration equation	R^2
CeBP	Positive	216.8	1.0×10^2	10.4%	14.5%	0.2 - 100	$y = 85.0x + 79.6$	0.998
	Negative	650.4	1.0×10^3	16.8%	20.2%	0.08 - 100	$y = 155.0x + 266.7$	0.998
μmBP	Positive	216.8	1.6×10^2	12.7%	17.0%	0.2 - 100	$y = 215.0x + 815.6$	0.994
	Negative	154.8	1.6×10^3	15.5%	22.0%	0.08 - 100	$y = 226.9x + 631.5$	0.997
QDBP	Positive	216.8	0.8	14.2%	23.9%	0.2 - 20	$y = 36.1x + 67.9$	0.991
	Negative	154.8	8	17.6%	23.3%	0.2 - 20	$y = 85.0x + 20.8$	0.998

[a] The m/z values of the MS peaks used in quantitative analysis.

[b] The LODs were measured based at the cascading decreased sample concentrations with a signal-to-noise ratio greater than 3.

[c] The shot-to-shot RSDs were measured based on 20 shots at different locations on the MALDI target (n = 20).

[d] The sample-to-sample RSDs were measured based on 15 samples in different batches (n = 15).

Table S2. Peaks detected and their intensities of BP by dual-ion-mode LDI-FTICR MS in Figure 1b-c.

Negative ion mode		Positive ion mode	
Peak	Peak intensity	Peak	Peak intensity
P_{13}^-	3.75×10^7	P_7^+	4.90×10^8
P_{15}^-	2.28×10^7	P_8^+	1.20×10^6
P_{17}^-	7.41×10^7	P_9^+	4.76×10^7
P_{21}^-	2.44×10^7	P_{10}^+	3.17×10^7
P_{23}^-	4.89×10^7	P_{11}^+	1.94×10^8
$[P_{18}H_2+Ce+K-2H]^-$	5.14×10^9	P_{12}^+	2.88×10^7
P_{25}^-	5.47×10^7	P_{13}^+	6.42×10^8
P_{27}^-	4.63×10^7	P_{14}^+	7.76×10^7
P_{29}^-	1.05×10^8	P_{15}^+	7.26×10^8
P_{31}^-	2.52×10^7	P_{16}^+	1.02×10^8
		P_{17}^+	5.08×10^8
		P_{18}^+	7.94×10^7
		P_{19}^+	5.87×10^8
		P_{20}^+	4.20×10^7
		P_{21}^+	6.80×10^8
		P_{22}^+	2.23×10^7
		P_{23}^+	7.13×10^8
		P_{24}^+	3.62×10^7
		P_{25}^+	6.21×10^8

Table S3. Peaks detected and their intensities of different BP materials by dual-ion-mode LDI-TOF MS in Figure 1d-m.

Negative ion mode

BP		OBP		μmBP		QDBP		CeBP	
Peak	Intensity	Peak	Intensity	Peak	Intensity	Peak	Intensity	Peak	Intensity
P_2^-	5336	PO_2^-	463	P_2^-	2366	P_2^-	440	P_3^-	356
P_3^-	4132	P_2HO^-	2741	P_3^-	3595	P_3^-	494	P_5^-	1825
P_5^-	16795	P_5^-	2962	P_5^-	29988	P_4^-	91	P_7^-	1507
P_6^-	3062	P_7^-	2616	P_6^-	2245	P_5^-	3104	P_8^-	700
P_7^-	12043	P_8^-	2777	P_7^-	19882	P_6^-	440	P_9^-	1436
P_8^-	7799	P_9^-	3668	P_8^-	9298	P_7^-	1129	P_{10}^-	693
P_9^-	10711	P_{10}^-	3793	P_9^-	17341	P_8^-	275	P_{11}^-	903
P_{10}^-	6917	P_{11}^-	3629	P_{10}^-	7977	P_9^-	909	P_{12}^-	251
P_{11}^-	6126	$P_{11}O_2^-$	2939	P_{11}^-	7484	P_{10}^-	237	P_{13}^-	2348
P_{12}^-	2558	$P_{12}O_2^-$	6863	P_{12}^-	1743	P_{11}^-	278	P_{15}^-	1618
P_{13}^-	12966	$P_{14}O_2^-$	7220	P_{13}^-	23312	P_{12}^-	172	P_{17}^-	2785
P_{14}^-	1410	$P_{15}O_2^-$	3297	P_{14}^-	1245	P_{13}^-	981	P_{19}^-	460
P_{15}^-	8832	$P_{16}O_2^-$	10850	P_{15}^-	16629	P_{14}^-	110	P_{21}^-	2505
P_{16}^-	3650	$P_{18}O_2^-$	3668	P_{16}^-	1928	P_{15}^-	382	P_{23}^-	773
P_{17}^-	10455	$[P_{17}H_2O_2+K-2H]^-$	6451	P_{17}^-	22718	P_{17}^-	928	$[P_{15}H_2+Na-2H]^-$	3555
P_{18}^-	833	$P_{19}HO_2^-$	1073	P_{18}^-	219	P_{19}^-	42	$[P_{19}H_2O]^-$	5101
P_{19}^-	2332	$P_{20}O_2^-$	2094	P_{19}^-	2467	P_{20}^-	22	$[P_{18}H_2+Ce+K-2H]^-$	18973
P_{20}^-	209	$P_{20}O_3^-$	566	P_{20}^-	310	P_{22}^-	22	$[P_4H_4+Na-2H]^-$	4791

P_{21}^-	1812	$P_{21}HO_2^-$	618	P_{21}^-	902	P_{23}^-	94		
P_{22}^-	153	$P_{22}O_2^-$	5689	P_{23}^-	3841	P_{24}^-	23		
P_{23}^-	3579	$P_{22}O_3^-$	395	P_{25}^-	861	$[P_2H_3+K-2H]^-$	1601		
P_{24}^-	222	$P_{23}HO_2^-$	879	P_{27}^-	313	$[P_4H_2+Na-2H]^-$	1103		
P_{25}^-	1691	$P_{24}O_2^-$	1815	P_{29}^-	1123	$[P_4H_4+K-2H]^-$	313		
P_{27}^-	781	$P_{28}HO_2^-$	1465	$[P_2H_3+K-2H]^-$	5868	$[P_6H_4+K-2H]^-$	482		
P_{29}^-	1326	$P_{26}HO_2^-$	828	$[P_4H_2+Na-2H]^-$	2961				
P_{31}^-	236			$[P_{10}H_3+K-2H]^-$	1335				
				$[P_{12}H_3+K-2H]^-$	941				
				$[P_{14}H_3+K-2H]^-$	1383				
Positive ion mode									
P_3^+	22762	P_3^+	9423	P_3^+	6316	P_3^+	92	P_3^+	935
P_4^+	26459	P_3O^+	7904	P_4^+	8897	P_4^+	225	P_4^+	1121
P_5^+	27553	P_5^+	12554	P_5^+	12247	P_5^+	186	P_5^+	3119
P_6^+	18930	P_6^+	8600	P_6^+	3601	P_7^+	1145	P_6^+	491
P_7^+	38262	P_7^+	18102	P_7^+	26389	P_8^+	74	P_7^+	17007
P_8^+	19705	P_7O^+	5549	P_8^+	3212	P_9^+	76	P_8^+	830
P_9^+	22199	P_8^+	8739	P_9^+	6486	P_{11}^+	46	P_9^+	2119
P_{10}^+	15012	P_9^+	9633	P_{10}^+	2015	P_{13}^+	104	P_{10}^+	585
P_{11}^+	19142	P_{10}^+	6739	P_{11}^+	4513	P_{15}^+	32	P_{11}^+	1392
P_{12}^+	4535	$[P_{10}+Na]^+$	5159	P_{12}^+	379	Na	183	P_{12}^+	129

P_{13}^+	21498	P_{11}^+	10981	P_{13}^+	5312	K	980	P_{13}^+	1975
P_{14}^+	5996	$P_{11}O^+$	3184	P_{14}^+	402	$[P_2H+Na]^+$	131	P_{14}^+	303
P_{15}^+	14722	P_{12}^+	3152	P_{15}^+	1913	$[PH_2N_2+K]^+$	2629	P_{15}^+	1141
$P_{15}O_2^+$	2839	P_{13}^+	8985	P_{16}^+	247	$[P_2N_2+Na]^+$	4101	P_{17}^+	407
P_{17}^+	8706	P_{14}^+	4289	P_{17}^+	779	$P_3H_2O_2^+$	2035	P_{19}^+	793
P_{18}^+	1162	P_{15}^+	7632	P_{19}^+	1258			$[P_{16}+Ce]^+$	4314
P_{19}^+	10978	P_{16}^+	2398	P_{21}^+	1316			P_{21}^+	706
P_{20}^+	1487	P_{17}^+	5971	P_{23}^+	1947			P_{23}^+	1118
P_{21}^+	11256	P_{18}^+	1028	P_{25}^+	2389			P_{25}^+	1128
P_{23}^+	10889	P_{19}^+	6906	Na	1117			Na	442
P_{25}^+	9676	P_{20}^+	455	K	5314			K	2215
		P_{21}^+	6977	$[P_2H+Na]^+$	3956			$[P_2H+Na]^+$	2135
		P_{23}^+	6155	$[PH_2N_2+K]^+$	30749			$[PH_2N_2+K]^+$	8263
		Na	8166	$P_3H_2O_2^+$	15045			$[P_2N_2+Na]^+$	23552
		K	22659						
		$[P_2H+Na]^+$	1902						
		$P_{12}H_2O_3^+$	4212						
		$P_{13}H_3O_3^+$	2337						
		$P_{14}H_3O_3^+$	4401						
		$P_{15}H_3O_3^+$	1063						
		$P_{17}H_2O_3^+$	638						

32

Table S4. The intensities, repeatability, and mass errors of typical peaks of BP during degradation in Figure 2a and Table S2.

Peak	0 d	2 d	4 d	8 d	12 d	20 d	Sample-to-sample RSD (n = 15)[a]	Measured *m/z*	Theoretical *m/z*	Mass error (ppm)
$[PO_2+Na]^+$	231	652	722	680	1778	391	5.1%	85.954	85.952	17
$P_4O_2^+$	0	228	5968	10937	11631	16052	20.4%	155.888	155.884	21
$[P_7O_2+Na]^+$	286	501	990	2051	829	455	8.9%	271.793	271.795	-8
$[P_8O_2+2Na]^+$	1126	454	0	1003	1526	0	22.4%	325.765	325.759	19
$P_{23}O_2^+$	80	225	183	174	186	0	11.8%	744.379	744.386	-8
$[PH_2O_2+Na]^+$	202	554	296	1274	888	592	4.0%	87.967	87.968	-14
$[PH_2O_3+Na]^+$	391	188	2225	2714	8998	816	14.7%	117.937	117.934	21
$[P_2HO_2+Na]^+$	121	261	378	422	749	679	4.9%	103.965	103.963	17
$P_2H_2O_3^+$	173	388	0	395	374	400	2.8%	111.945	111.947	-18
$[P_5H_2O_3+Na]^+$	384	631	598	1086	788	0	15.1%	227.850	227.858	-37
$[P_6HO_2+Na]^+$	828	1057	1377	5571	1864	788	28.4%	241.834	241.829	20
$[P_7H_2O_2+Na]^+$	344	1110	1122	2483	1407	555	13.8%	273.813	273.811	-6
$[P_3H_4O_4+K]^+$	0	228	5968	10937	11631	16052	7.0%	199.907	199.904	18
$P_8H_2O_3^+$	613	693	955	1294	913	0	7.8%	297.793	297.790	12
$P_9HO_2^+$	3202	2259	1851	1932	1770	0	4.4%	311.765	311.761	13
$P_9HO_3^+$	616	1222	1542	1794	1339	0	20.8%	327.763	327.756	23
$P_{10}H_2O_2^+$	525	1189	719	3178	937	0	22.7%	343.750	343.743	22
$P_{10}H_2O_3^+$	549	1846	1913	1746	1179	0	4.6%	359.750	359.737	36
$P_{11}H_2O_3^+$	155	566	710	648	310	0	4.7%	390.700	390.711	-29
$P_{12}H_2O_3^+$	817	3018	3530	4010	2387	210	14.1%	421.693	421.685	20
$P_{13}H_2O_3^+$	187	842	1083	1927	741	0	25.8%	452.653	452.659	-13

$P_9N_4^+$	2392	1829	3797	2700	2345	388	7.8%	334.770	334.776	-18
$P_{10}N_2^+$	3082	2113	5105	3473	3115	516	6.7%	337.750	337.743	20
$P_{18}N_2^+$	113	607	763	344	370	0	12.9%	585.523	585.533	-18
$[P_7N_2+K]^+$	932	3312	1898	5565	3896	553	8.1%	283.792	283.786	21
$[P_9N_2+2Na]^+$	27238	21058	34689	32070	17707	4058	12.1%	352.746	352.749	-7
$[P_{14}N_2+Na]^+$	795	2479	2579	4138	1985	180	10.0%	484.625	484.628	-7
$[P_{15}N_2+Na]^+$	118	305	327	833	0	0	4.6%	515.593	515.602	-17
$[P_{16}N_2+Na]^+$	475	1739	1698	3322	1313	91	14.8%	546.566	546.576	-18
$[P_{18}N_2+Na]^+$	251	636	456	1068	515	0	17.1%	608.513	608.523	-17
$[P_{22}N_2+Na]^+$	91	238	241	511	358	0	4.4%	732.408	732.418	-13
$[PH_2N_2+Na]^+$	481	311	424	366	563	466	14.7%	83.950	83.98	-59
$[PH_2N_2+K]^+$	311	1389	1832	503	505	390	1.6%	99.960	99.959	16
$[PN_2O_2+K]^+$	96	389	499	339	277	1093	20.0%	129.931	129.933	-17
$P_2H_4N_2O_4^+$	0	361	3397	7306	0	0	1.4%	157.966	157.964	10
$P_5N_2O_2^+$	0	843	1627	0	0	0	8.3%	214.868	214.864	19
$P_5N_4O_4^+$	603	0	1257	801	622	616	1.6%	274.866	274.860	21
$[P_5N_2O_2+K]^+$	0	682	797	1987	742	0	7.8%	253.850	253.828	88
$[P_6HN_2O_2+K]^+$	569	823	0	3057	0	374	11.8%	285.811	269.836	5
$[P_6HN_2O_2+Na]^+$	297	974	1480	2345	1224	379	11.4%	269.851	285.810	58
$[P_7H_2N_2O_2+Na]^+$	0	0	0	1644	0	303	11.8%	301.822	301.817	16
$[P_7N_2O_2+Na]^+$	1879	4281	4188	11785	3823	1089	5.9%	299.807	299.802	18
$[P_8N_2O_2+2Na]^+$	9899	11781	12797	10794	0	933	13.3%	353.766	353.765	2
$[P_{10}+Na]^+$	1898	911	2552	2044	1451	508	15.8%	332.732	332.727	16
$[P_9+K]^+$	844	430	0	1312	742	0	11.5%	317.750	317.727	72

$[P_7+K]^+$	7576	5655	8818	16318	7636	1482	7.2%	255.783	255.779	14
$[P_3+K]^+$	273	350	1139	0	517	0	11.1%	131.881	131.884	-26
$[PH_2+K]^+$	240	248	263	435	441	0	3.3%	71.953	71.953	6
$[P+K]^+$	653	799	640	1199	1349	643	13.1%	69.950	69.937	187
P_{25}^+	5617	4848	4522	5997	4341	364	5.6%	774.338	774.343	-7
P_{23}^+	4871	5789	6023	7493	4595	376	5.9%	712.393	712.396	-4
P_{21}^+	5017	5510	7044	8669	3460	388	10.8%	650.439	650.448	-14
P_{19}^+	4952	5097	7294	8218	3415	262	6.4%	588.510	588.501	15
P_{17}^+	3561	3368	5362	5320	1121	231	0.5%	526.549	526.553	-8
P_{16}^+	1235	1136	1469	1302	94	0	12.8%	495.581	495.580	3
P_{15}^+	6800	6487	9033	8702	1242	408	3.1%	464.603	464.606	-6
P_{14}^+	2357	1965	2486	2429	170	200	11.2%	433.628	433.632	-9
P_{13}^+	10474	10614	12570	11095	6688	776	8.9%	402.663	402.658	12
P_{12}^+	1517	1293	1467	1063	38	0	15.9%	371.691	371.685	17
P_{11}^+	9885	8059	9070	7253	2049	635	6.3%	340.706	340.711	-14
P_{10}^+	6165	5313	6689	4652	828	461	12.6%	309.729	309.737	-26
P_9^+	11638	10392	11638	9409	3145	1080	10.7%	278.767	278.763	13
P_8^+	9744	7715	9628	6615	1408	621	5.6%	247.791	247.790	6
P_7^+	26844	35170	34658	35326	7286	3543	1.0%	216.818	216.816	10
P_6^+	7284	7434	9099	6852	1315	813	4.1%	185.839	185.842	-16
P_5^+	17632	16782	18804	15707	12850	0	9.2%	154.870	154.868	11
P_4^+	17311	15071	16693	14553	8584	1681	7.3%	123.892	123.894	-20
P_3^+	8135	7987	6940	5481	1269	1373	4.4%	92.922	92.920	13

[a] The sample-to-sample RSDs were measured based on 15 samples in different batches (n = 15).

Table S5. The repeatability of typical ion ratios detected during BP degradation by LDI-MS (Fig. 2b-c).

Peak ratio	Sample-to-sample RSD (n = 15)[a]	Peak ratio	Sample-to-sample RSD (n = 15)[a]
$[P_7O_2+Na]/P_7$	13.1%	$P_4/[P_5H_2O_3+Na]$	10.0%
$[P_7H_2O_2+Na]/P_7$	5.6%	$P_7/[P_8H_2O_3]$	1.4%
$[P_7H_2O_2+Na]/[P_7O_2+Na]$	0.7%	$P_8/[P_9HO_3]$	4.5%
$[P_9HO_3]/[P_9HO_2]$	10.6%	$P_9/[P_{10}H_2O_3]$	5.6%
$P_8/[P_9HO_2]$	7.2%	$P_{10}/[P_{11}H_2O_3]$	1.6%
$[P_7N_2+K]/P_7$	2.7%	$P_{11}/[P_{12}H_2O_3]$	5.6%
$[P_7N_2O_2+Na]/[P_7N_2+K]$	4.5%	$P_{12}/[P_{13}H_2O_3]$	16.4%
$[P_7H_2N_2O_2+Na]/[P_7N_2+K]$	18.5%		
$[P_7H_2N_2O_2+Na]/[P_7N_2O_2+Na]$	0.7%		
$[P_7N_2+K]/[P_8N_2O_2+2Na]$	5.0%		

[a] The sample-to-sample RSDs were measured based on 15 samples in different batches (n = 15).

Table S6. Feature MS peaks and peak ratios in Fig. 2 used to deduce different degradation pathways in Fig. 3.[a]

Route 1	$[P_7H_2O_2+Na]/P_7$, $P_8/[P_9HO_2]$, $[PH_2O_2+Na]^+$, $[P_7H_2O_2+Na]^+$, $P_9HO_2^+$, $P_{10}H_2O_2^+$
Route 2	$[P_7O_2+Na]/P_7$, $[P_7H_2O_2+Na]/[P_7O_2+Na]$, $[PO_2+Na]^+$, $P_4O_2^+$, $[P_3H_4O_4+K]^+$, $[P_7O_2+Na]^+$, $[P_8O_2+2Na]^+$, $P_9HO_2^+$, $P_{23}O_2^+$
Route 3	$[P_9HO_3]/[P_9HO_2]$, $P_4/[P_5H_2O_3+Na]$, $P_7/[P_8H_2O_3]$, $P_8/[P_9HO_3]$, $P_9/[P_{10}H_2O_3]$, $P_{10}/[P_{11}H_2O_3]$, $P_{11}/[P_{12}H_2O_3]$, $P_{12}/[P_{13}H_2O_3]$, $[P_2HO_2+Na]^+$, $[PH_2O_3+Na]^+$, $P_2H_2O_3^+$, $[P_5H_2O_3+Na]^+$, $[P_5H_2O_3+Na]^+$, $[P_6HO_2+Na]^+$, $P_8H_2O_3^+$, $P_9HO_2^+$, $P_9HO_3^+$, $P_{10}H_2O_3^+$, $P_{11}H_2O_3^+$, $P_{12}H_2O_3^+$, $P_{13}H_2O_3^+$
Route 4	$[P_7N_2+K]/P_7$, $P_9N_4^+$, $P_{10}N_2^+$, $P_{18}N_2^+$, $[P_7N_2+K]^+$, $[P_9N_2+2Na]^+$, $[P_{14}N_2+Na]^+$, $[P_{15}N_2+Na]^+$, $[P_{16}N_2+Na]^+$, $[P_{18}N_2+Na]^+$, $[P_{22}N_2+Na]^+$, $P_2H_4N_2O_4^+$, $[P_7H_2N_2O_2+Na]^+$
Route 5	$[P_7N_2+K]/P_7$, $[P_7H_2N_2O_2+Na]/[P_7N_2+K]$, $[P_7H_2N_2O_2+Na]/[P_7N_2O_2+Na]$, $P_9N_4^+$, $P_{10}N_2^+$, $P_{18}N_2^+$, $[P_7N_2+K]^+$, $[P_9N_2+2Na]^+$, $[P_{14}N_2+Na]^+$, $[P_{15}N_2+Na]^+$, $[P_{16}N_2+Na]^+$, $[P_{18}N_2+Na]^+$, $[P_{22}N_2+Na]^+$, $[P_6HN_2O_2+Na]^+$
Route 6	$[P_7N_2+K]/P_7$, $[P_7N_2O_2+Na]/[P_7N_2+K]$, $[P_7N_2+K]/[P_8N_2O_2+2Na]$, $P_9N_4^+$, $P_{10}N_2^+$, $P_{18}N_2^+$, $[P_7N_2+K]^+$, $[P_9N_2+2Na]^+$, $[P_{14}N_2+Na]^+$, $[P_{15}N_2+Na]^+$, $[P_{16}N_2+Na]^+$, $[P_{18}N_2+Na]^+$, $[P_{22}N_2+Na]^+$, $[PN_2O_2+K]^+$, $P_5N_2O_2^+$, $P_5N_4O_4^+$, $[P_5N_2O_2+K]^+$, $[P_7N_2O_2+Na]^+$, $[P_8N_2O_2+2Na]^+$

[a] Here the MS signals are described in two different ways (i.e., peaks and peak ratios). The fingerprint peaks were used to identify key intermediates and products, and the peak ratios of the adjacent fingerprint peaks were mainly used to deduce the degradation pathways.

Table S7. Feature MS peaks by high-resolution LDI-FTICR MS verifying the different degradation pathways in Fig. 3.

Route 1	$P_{10}HO_2^+$ (342.7348, 0.15 ppm), $P_9H_2O_2^-$ (312.7687, -0.16 ppm), $P_2H_2O_2^+$ (95.9525, 0.11 ppm), $P_{11}H_2O_2^+$ (374.7163, 0.10 ppm), $P_{19}H_2O_2^+$ (622.5063, 0.16 ppm), $[P_{17}H_3O_2+K-2H]^-$ (598.5149, 0.20 ppm), $P_8HO_3^-$(296.7821, -0.18 ppm), $P_{10}H_3O_3^-$ (360.7453, -0.06 ppm), $P_{11}H_2O_3^-$ (390.7112, -0.04 ppm), $P_4H_2O_3^+$ (173.8949, -0.13 ppm), $P_{11}H_2O_3^+$ (390.7113, 0.07 ppm), $P_{12}H_2O_3^+$ (421.6849, -0.20 ppm), $P_{13}H_3O_3^+$ (453.6667, 0.18 ppm)
Route 2	$P_9O_2^-$ (310.7532, 0.17 ppm), $P_{11}O_2^+$ (372.7006, -0.16 ppm), $P_{15}O_2^-$ (496.5958, 0.19 ppm), $P_{19}O_2^+$ (620.4906, -0.17 ppm), P_6O^- (201.8369, -0.20 ppm), $P_{11}O^+$ (356.7058, 0.18 ppm), $P_{13}O^-$ (418.6534, 0.20 ppm), $P_{20}O^+$ (635.4697, 0.19 ppm), $P_{12}HO^-$(388.6874, 0.13 ppm), $P_{10}HO_2^+$ (342.7348, 0.15 ppm), $P_2H_2O_2^+$ (95.9525, 0.11 ppm), $P_9H_2O_2^-$ (312.7687, -0.16 ppm), $P_{11}H_2O_2^+$ (374.7163, 0.10 ppm), $P_{19}H_2O_2^+$ (622.5063, 0.16 ppm), $[P_{17}H_3O_2+K-2H]^-$ (598.5149, 0.20 ppm), $P_8HO_3^-$ (296.7821, -0.18 ppm), $P_{10}H_3O_3^-$ (360.7453, -0.06 ppm), $P_{11}H_2O_3^-$ (390.7112, -0.04 ppm), $P_4H_2O_3^+$ (173.8949, -0.13 ppm), $P_{11}H_2O_3^+$ (390.7113, 0.07 ppm), $P_{12}H_2O_3^+$ (421.6849, -0.20 ppm), $P_{13}H_3O_3^+$ (453.6667, 0.18 ppm)
Route 3	$P_9O_2^-$ (310.7532, 0.17 ppm), $P_{11}O_2^+$ (372.7006, -0.16 ppm), $P_{15}O_2^-$ (496.5958, 0.19 ppm), $P_{19}O_2^+$ (620.4906, -0.17 ppm), $P_{10}HO_2^+$ (342.7348, 0.15 ppm), $P_8HO_3^-$ (296.7821, -0.18 ppm), $P_{10}H_3O_3^-$ (360.7453, -0.06 ppm), $P_{11}H_2O_3^-$ (390.7112, -0.04 ppm), $P_4H_2O_3^+$ (173.8949, -0.13 ppm), $P_{11}H_2O_3^+$ (390.7113, 0.07 ppm), $P_{12}H_2O_3^+$ (421.6849, -0.20 ppm), $P_{13}H_3O_3^+$ (453.6667, 0.18 ppm), $P_8H_3O_4^-$ (314.7926, -0.10 ppm), $[P_{24}H_4O_4+Na-2H]^-$ (832.3547, -0.07 ppm)
Route 4	$[P_{21}N_2+K]^+$ (717.4184, 0.14 ppm), $[P_{21}N_2+2Na]^+$ (724.4342, 0.09 ppm), $[P_8H_2N_2+Na-2H]^-$ (329.7593, 0.09 ppm), $[P_5N_2+Na]^+$ (205.8641, -0.14 ppm), $P_{25}N_2O_2^-$ (834.3393, -0.20 ppm), $[P_3N_2O_2+K]^+$ (191.8804, -0.16 ppm), $[P_7N_2O_2+2Na]^+$ (322.7915, 0.62 ppm), $[P_{10}N_2O_2+Na]^+$ (392.7229, 0.14 ppm), $[P_{11}N_2O_2+Na]^+$ (423.6965, -0.10 ppm), $P_5HN_2O_2^+$ (215.8720, -0.14 ppm), $P_{16}HN_2O_2^+$ (556.5836, 0.20 ppm), $[P_4HN_2O_2+Na]^+$ (207.8880, -

	0.14 ppm), $[P_{14}H_2N_2O_2+K\text{-}2H]^-$ (532.5917, -0.11 ppm), $[P_{16}H_2N_2O_2+K\text{-}2H]^-$ (594.5393, 0.03 ppm), $[P_{20}HN_2O_2+K]^+$ (719.4420, -0.20 ppm), $[P_7H_2N_2O_2+Na]^+$ (301.8171, -0.10 ppm), $[P_7H_3N_2O_2+K\text{-}2H]^-$ (316.7833, 0.14 ppm), $[P_9H_3N_2O_2+Na\text{-}2H]^-$ (362.7568, -0.09 ppm), $P_9N_2O_3^+$ (354.754, -0.15 ppm), $P_{11}N_2O_3^-$ (416.7018, 0.19 ppm), $P_{15}N_2O_3^+$ (540.5967, -0.13 ppm), $P_9H_2N_2O_3^-$ (356.7699, 0.06 ppm)
Route 5	$[P_{21}N_2+K]^+$ (717.4184, 0.14 ppm), $[P_{21}N_2+2Na]^+$ (724.4342, 0.09 ppm), $[P_8H_2N_2+Na\text{-}2H]^-$ (329.7593, 0.09 ppm), $[P_5N_2+Na]^+$ (205.8641, -0.14 ppm), $P_{25}N_2O_2^-$ (834.3393, -0.20 ppm), $[P_3N_2O_2+K]^+$ (191.8804, -0.16 ppm), $[P_7N_2O_2+2Na]^+$ (322.7915, 0.62 ppm), $[P_{10}N_2O_2+Na]^+$ (392.7229, 0.14 ppm), $[P_{11}N_2O_2+Na]^+$ (423.6965, -0.10 ppm), $P_5HN_2O_2^+$ (215.8720, -0.14 ppm), $P_{16}HN_2O_2^+$ (556.5836, 0.20 ppm), $[P_4HN_2O_2+Na]^+$ (207.8880, -0.14 ppm), $[P_{14}H_2N_2O_2+K\text{-}2H]^-$ (532.5917, -0.11 ppm), $[P_{16}H_2N_2O_2+K\text{-}2H]^-$ (594.5393, 0.03 ppm), $[P_{20}HN_2O_2+K]^+$ (719.4420, -0.20 ppm), $[P_7H_2N_2O_2+Na]^+$ (301.8171, -0.10 ppm), $[P_9H_3N_2O_2+Na\text{-}2H]^-$ (362.7568, -0.09 ppm), $[P_7H_3N_2O_2+K\text{-}2H]^-$ (316.7833, 0.14 ppm), $P_9N_2O_3^+$ (354.754, -0.15 ppm), $P_{11}N_2O_3^-$ (416.7018, 0.19 ppm), $P_{15}N_2O_3^+$ (540.5967, -0.13 ppm), $P_9H_2N_2O_3^-$ (356.7699, 0.06 ppm)
Route 6	$[P_5N_2+Na]^+$ (205.8641, -0.14 ppm), $[P_{21}N_2+K]^+$ (717.4184, 0.14 ppm), $[P_{21}N_2+2Na]^+$ (724.4342, 0.09 ppm), $[P_8H_2N_2+Na\text{-}2H]^-$ (329.7593, 0.09 ppm), $P_{25}N_2O_2^-$ (834.3393, -0.20 ppm), $[P_3N_2O_2+K]^+$ (191.8804, -0.16 ppm), $[P_7N_2O_2+2Na]^+$ (322.7915, 0.62 ppm), $[P_{10}N_2O_2+Na]^+$ (392.7229, 0.14 ppm), $[P_{11}N_2O_2+Na]^+$ (423.6965, -0.10 ppm), $P_5HN_2O_2^+$ (215.8720, -0.14 ppm), $P_{16}HN_2O_2^+$ (556.5836, 0.20 ppm), $[P_4HN_2O_2+Na]^+$ (207.8880, -0.14 ppm), $[P_7H_2N_2O_2+Na]^+$ (301.8171, -0.10 ppm), $[P_7H_3N_2O_2+K\text{-}2H]^-$ (316.7833, 0.14 ppm), $[P_9H_3N_2O_2+Na\text{-}2H]^-$ (362.7568, -0.09 ppm), $[P_{14}H_2N_2O_2+K\text{-}2H]^-$ (532.5917, -0.11 ppm), $[P_{16}H_2N_2O_2+K\text{-}2H]^-$ (594.5393, 0.03 ppm), $[P_{20}HN_2O_2+K]^+$ (719.4420, -0.20 ppm)

48

Table S8. Detailed parameters of DFT and molecular dynamic model in Fig. S13.

	total/eV	P/eV	N_2/eV	E_abs/eV
P-N_2	-209.70	-193.09	-16.95	0.33

3. Supplementary Figures

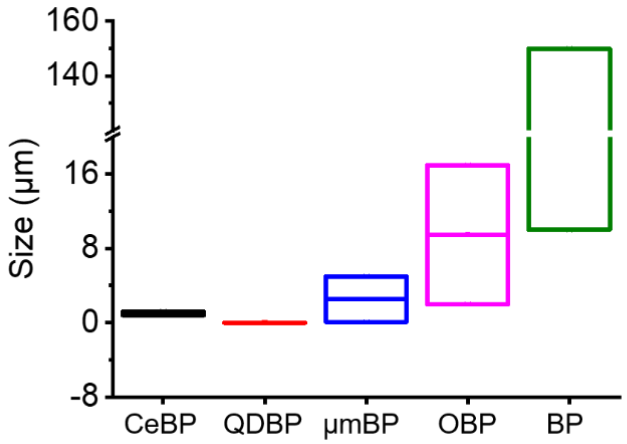

Figure S1. Rough estimate of particle size of the BP materials used in this study. The particle size was in the order of BP > OBP > μmBP > CeBP> QDBP.

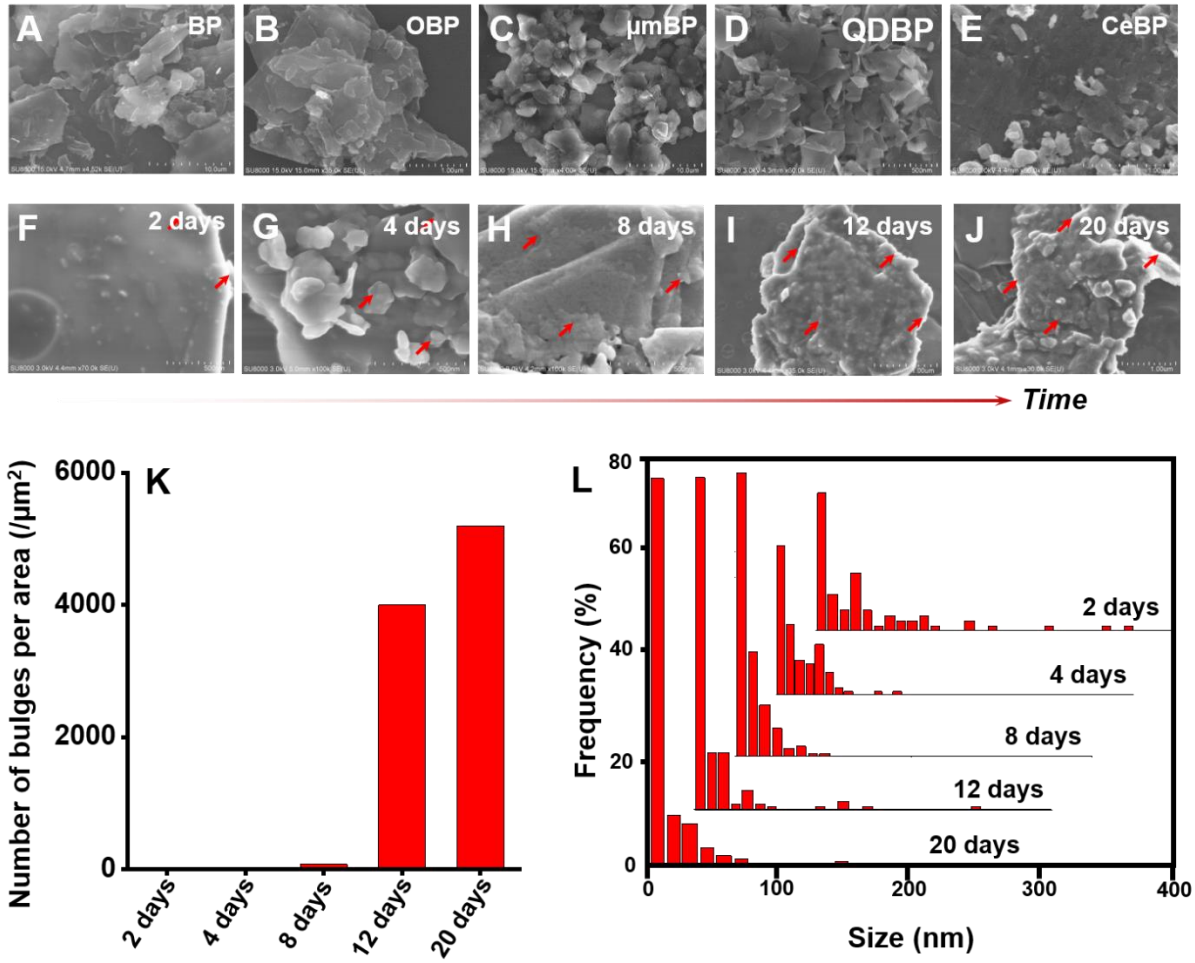

Figure S2. Typical SEM images showing the morphology of different BP materials and the morphological change during its degradation process. A-E, Typical SEM images of BP (**A**), OBP (**B**), μmBP (**C**), QDBP (**D**), and CeBP (**E**). **F-J**, Morphological change of BP during the degradation process up to 20 days. Time: **F**) 2 d, **G**) 4 d, **H**) 8 d, **I**) 12 d, and **J**) 20 d. **K**) The number of bulges per area observed on the surface of BP sheets (per μm^2 of BP surface). **L**) The statistic histogram of the relative frequency of bulges of different sizes. The statistic analysis of the SEM images was performed with the Image-Pro Plus software and 20 sample spots. It can be observed that with prolonging the incubation time, the number of bulges on the BP sheets increased obviously, and more small bulges with size less than 50 nm appeared. Similar phenomenon has also been observed previously.[1]

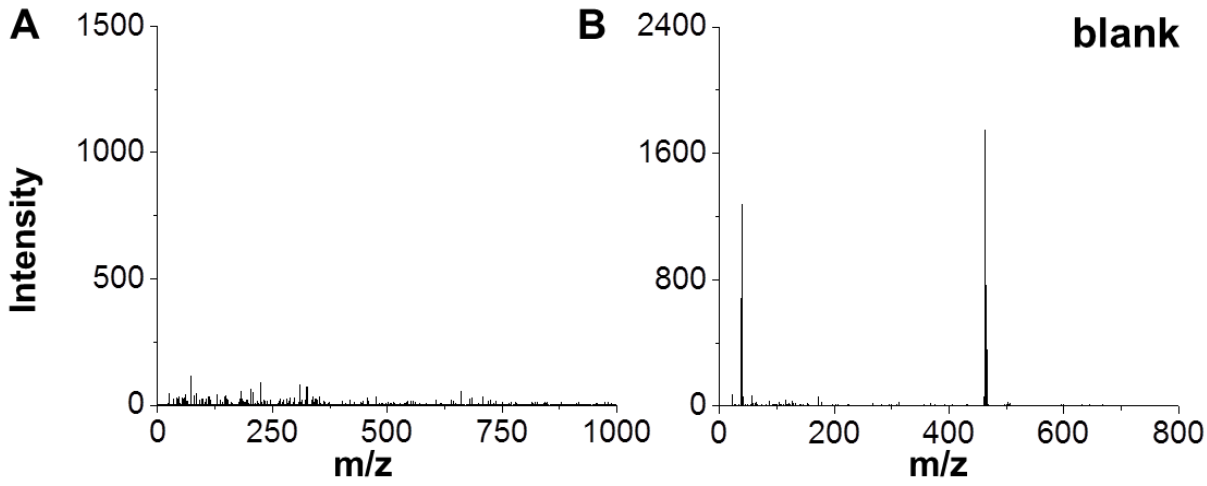

Figure S3. Mass spectra of blank samples in LDI-TOF MS. The left and right columns represent the spectra obtained in negative (**A**) and positive ion mode (**B**), respectively. It can be seen that the blank samples had no mass spectra signals corresponding to BP.

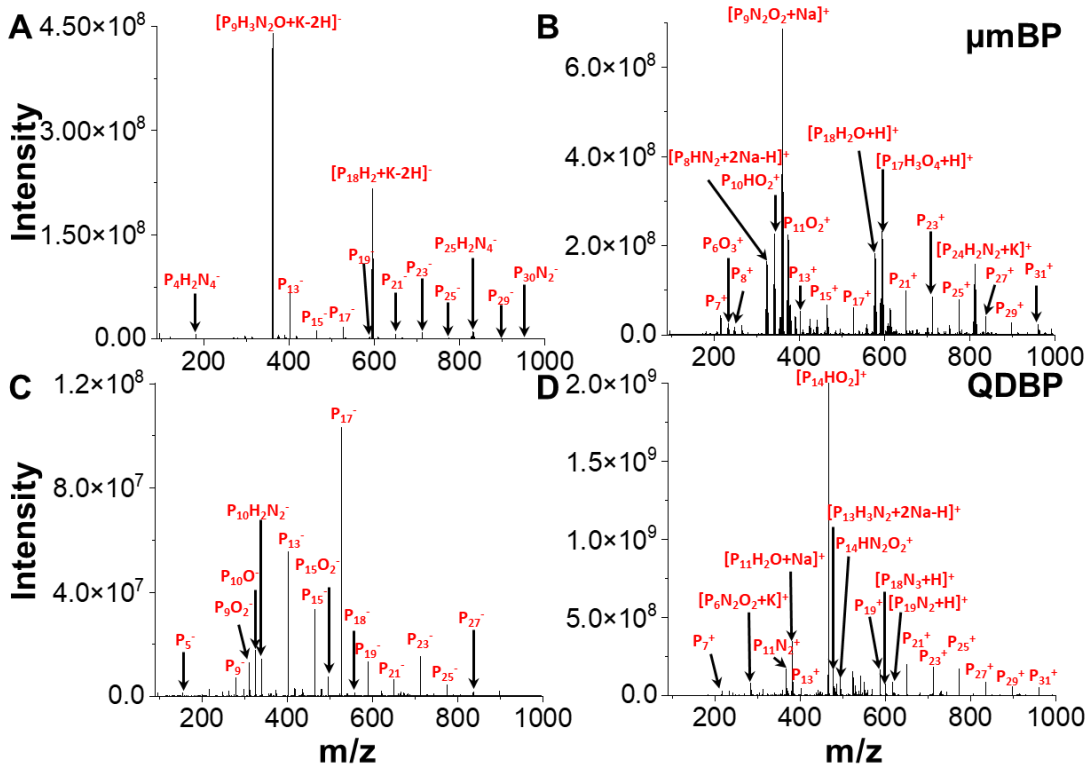

Figure S4. Mass spectra of μmBP and QDBP by dual-ion-mode LDI-FTICR MS. (**A, B**) μmBP, and (**C, D**) QDBP. The left and right columns represent the spectra obtained in negative and positive ion mode, respectively. Analyte concentration: 100 μg/mL. The mass spectra verified that the chemical functionalization of BP affected the MS fingerprints. For each spectrum, 20 shots were made in different sample regions and the spectrum with average intensities is shown to ensure the representativeness.

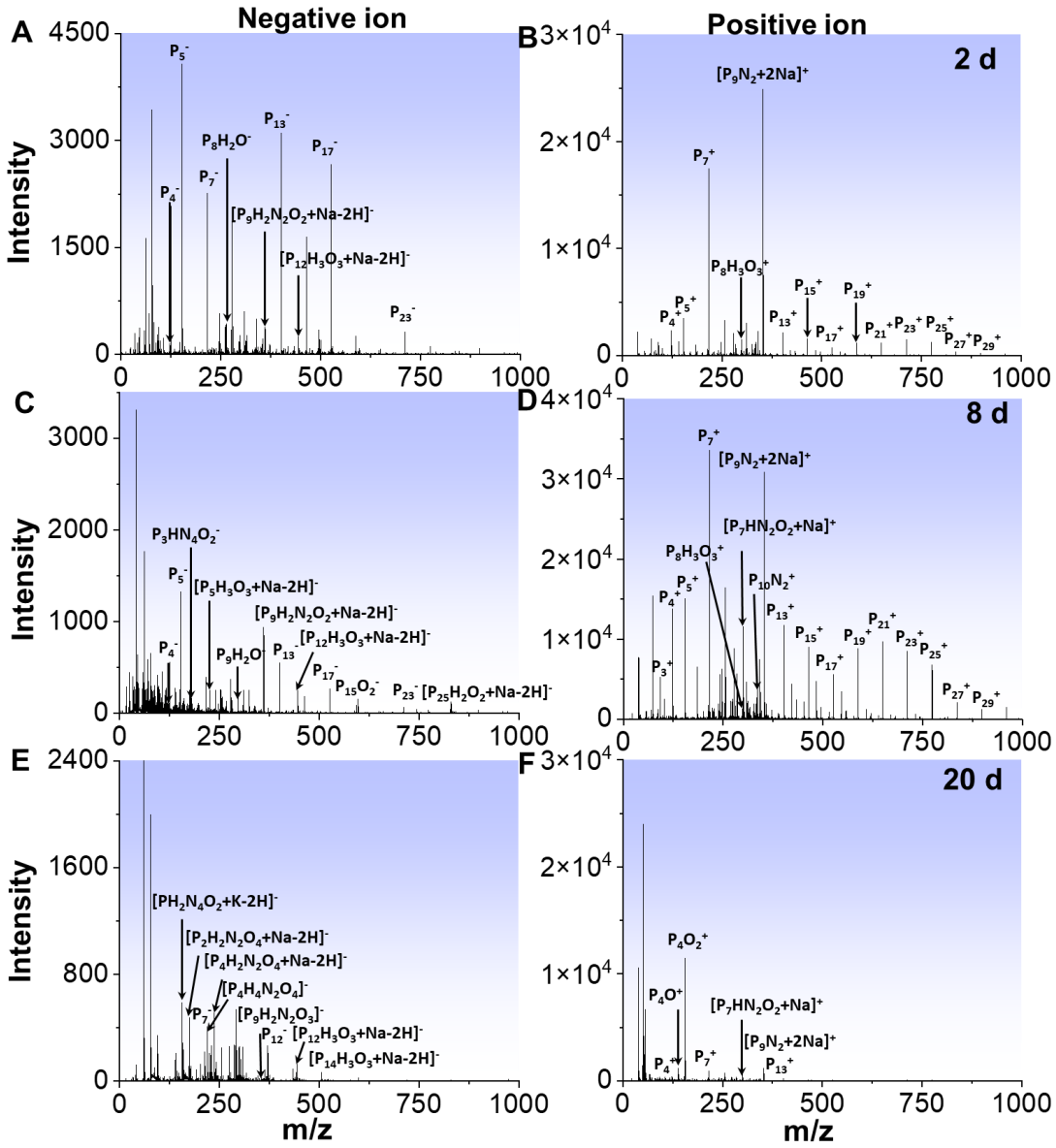

Figure S5. Monitoring the ambient stability of untreated BP by dual-ion-mode LDI-TOF MS. (**A, B**) 2 days, (**C, D**) 8 days, and (**E, F**) 20 days. The left and right columns represent the spectra obtained in the negative and positive ion mode, respectively. A variety of peaks of oxidized and nitrided products were yielded in the spectra with the peak intensities varying with the degradation time. For each spectrum, 20 shots were made in different sample regions and the spectrum with average intensities is shown to ensure the representativeness.

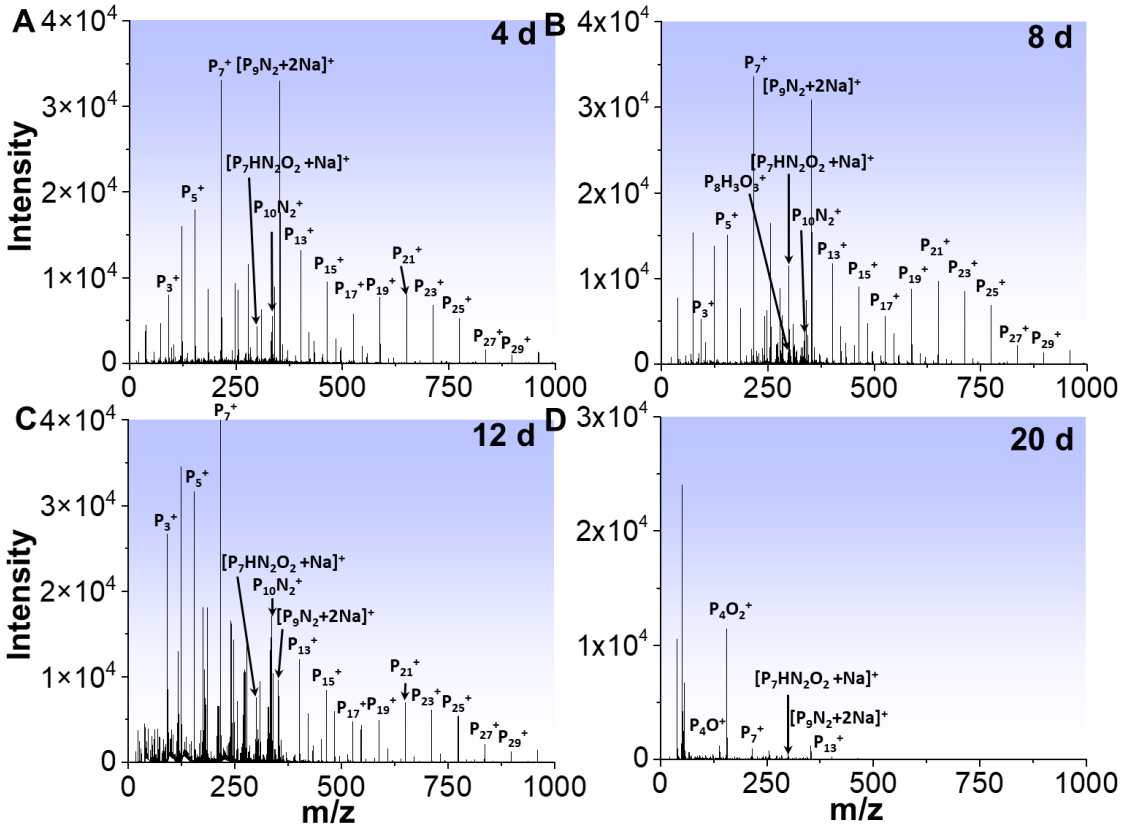

Figure S6. Monitoring the ambient stability of untreated BP by LDI-TOF MS at different time points. A) 4 days, **B**) 8 days, **C**) 12 days, and **D**) 20 days. The columns represent the spectra obtained in the positive ion mode. A variety of peaks of oxidized and nitrided products were yielded in the spectra with the peak intensities varying with the degradation time. The spectra corresponded to Figure 2. For each spectrum, 20 shots were made in different sample regions and the spectrum with average intensities is shown to ensure the representativeness.

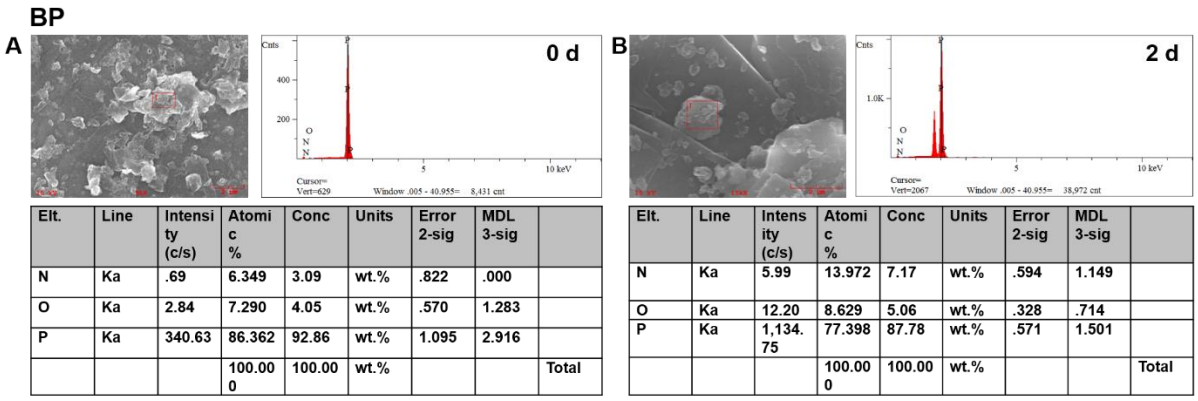

Elt.	Line	Intensity (c/s)	Atomic %	Conc	Units	Error 2-sig	MDL 3-sig	
N	Ka	.69	6.349	3.09	wt.%	.822	.000	
O	Ka	2.84	7.290	4.05	wt.%	.570	1.283	
P	Ka	340.63	86.362	92.86	wt.%	1.095	2.916	
			100.000	100.00	wt.%			Total

Elt.	Line	Intensity (c/s)	Atomic %	Conc	Units	Error 2-sig	MDL 3-sig	
N	Ka	5.99	13.972	7.17	wt.%	.594	1.149	
O	Ka	12.20	8.629	5.06	wt.%	.328	.714	
P	Ka	1,134.75	77.398	87.78	wt.%	.571	1.501	
			100.000	100.00	wt.%			Total

Elt.	Line	Intensity (c/s)	Atomic %	Conc	Units	Error 2-sig	MDL 3-sig	
N	Ka	6.03	9.596	5.17	wt.%	.455	1.112	
O	Ka	47.10	22.299	13.72	wt.%	.442	1.112	
P	Ka	1,339.13	68.105	81.11	wt.%	.481	1.279	
			100.000	100.00	wt.%			Total

Figure S7. EDX characterization of BP treated at different temperatures in air. The EDX patterns of BP were obtained at the highlighted sections in the SEM images and the elemental analysis results are also given. Incubation time: **A**) without incubation, **B**) 2 d, and **C**) 4 d. It can be seen that the atomic percentage of O in BP gradually increased, indicating the increasing generation of oxidized intermediates/products; meanwhile, the ratio of the atomic percentage of N to O increased first and then decreased, which probably resulted from the generation of nitride intermediates and then their detachment from the BP surface.

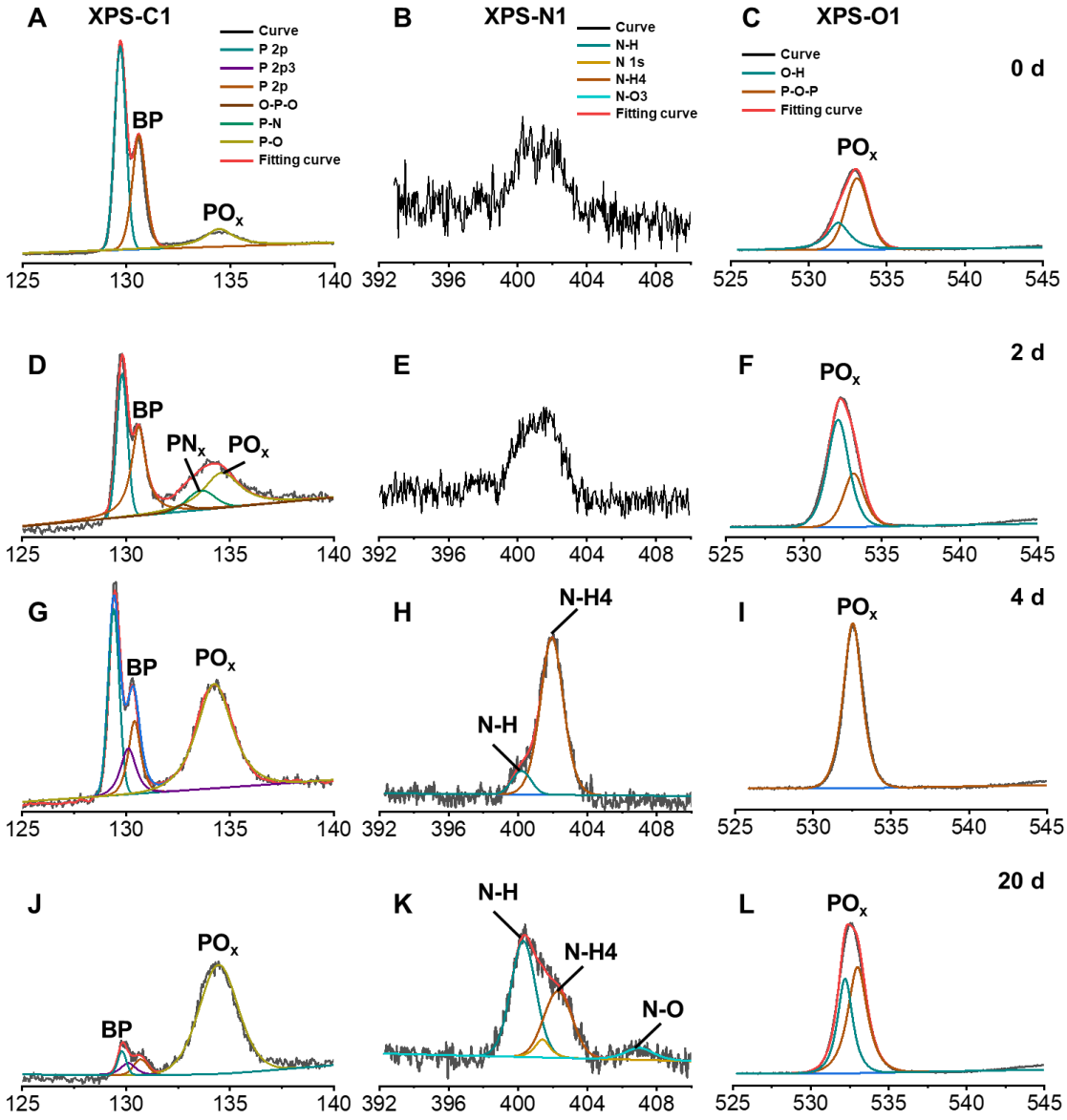

Figure S8. C1s, N1s, and O1s XPS spectra of BP in air over time. (**A, D, G, J**) C1s XPS spectra, (**B, E, H, K**) N1s XPS spectra, and (**C, F, I, L**) O1s XPS spectra. The incubation time was (**A-C**) 0 d, (**D-F**) 2 d, (**G-I**) 4 d, and (**J-L**) 20 d. The peaks at 132.4, 134.6, 135.8, and 133.4 eV are assigned to O-P-O, P-O, P-O, and P-N bonds, respectively. It can be seen that the P-N bond in BP gradually increased and then decreased with time, indicating the production of N-containing intermediates and their further dissociation from the BP surface. After degradation, the N1 XPS spectra exhibited that the peaks of -N-H-, -N-N-, and -N-O- bonds yielded, and the chemical bonds of -P-N-, -P=N-, -P-O-, and -P=O- appeared on the C1 XPS spectra. These peaks verified the formation of the key oxidation and N_2-addition oxidation intermediate ions.

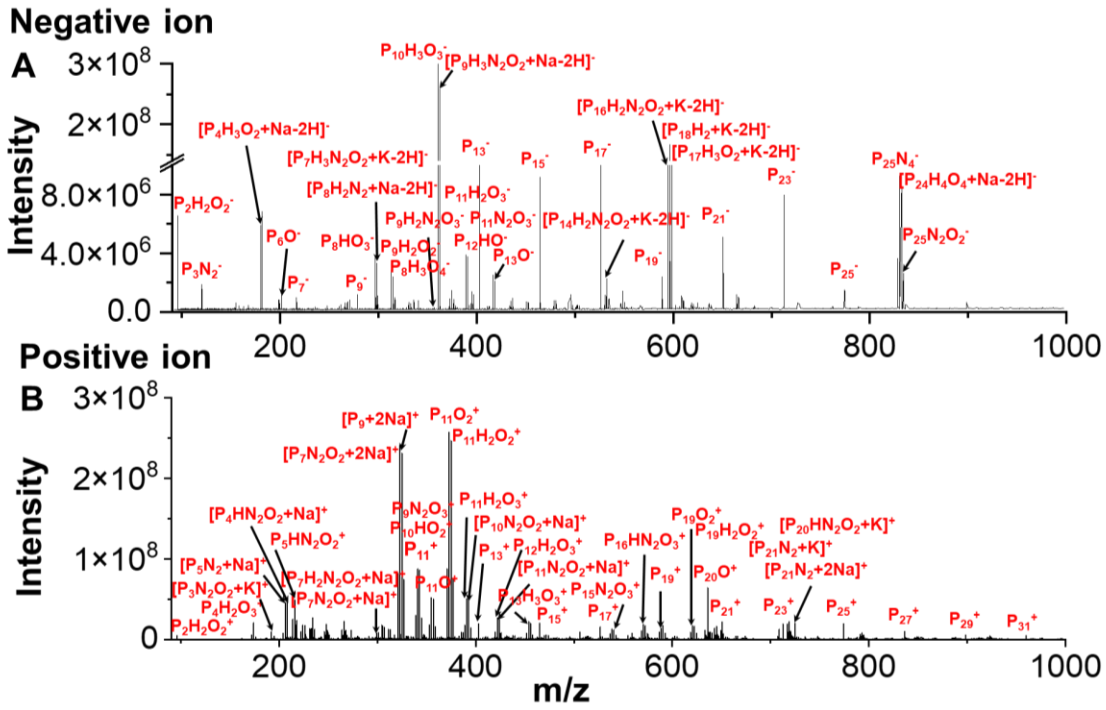

Figure S9. Monitoring the ambient stability of untreated BP by dual-ion-mode LDI-FTICR MS after degradation for 7 days. A and **B** represent typical spectra obtained in the negative and positive ion mode, respectively. After 7 days of degradation, a variety of peaks of oxidized and nitrided products were yielded in the spectra. Due to the high resolution (Table S3), the LDI-FTICR MS results well verified the results obtained by LDI-TOF MS. For each spectrum, 20 shots were made in different sample regions and the spectrum with average intensities is shown to ensure the representativeness.

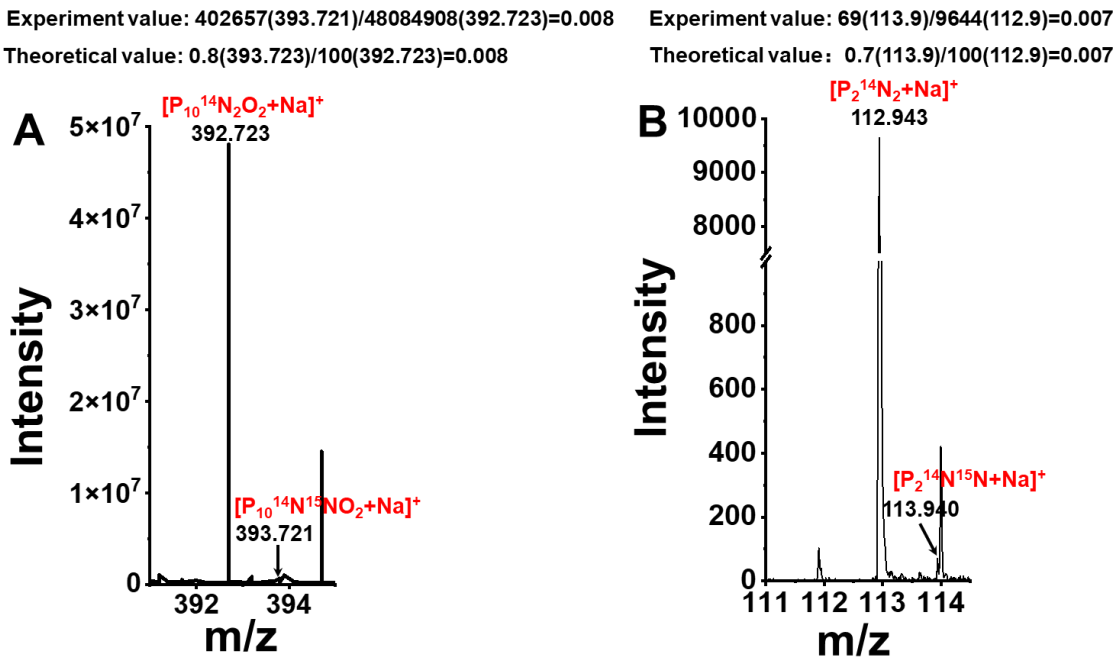

Figure S10. The stable nitrogen isotope patterns verifying the nitrided products during the BP degradation. The left and right column show the peaks of two nitrided products ([$P_{10}N_2O_2$+Na] and [P_2N_2+Na]) in positive-ion LDI-FTICR MS. Nitrogen has two natural stable isotopes (^{14}N and ^{15}N) with the abundance ratio of 99.634%:0.366%. The theoretical value of the nitrogen isotope patterns for the nitrided products was calculated by the Compass IsotopePattern Software (Bruker). It can be seen that the N isotope patterns could be observed for the identified nitrided products ([$P_{10}{}^{14}N^{15}NO_2$+Na]$^+$ and [$P_2{}^{14}N^{15}N$+Na]$^+$), and the experimental values of the nitrogen isotope patterns for the nitrided products were highly consistent with the theoretical values, indicating that the identified products were accurate. It is worth noting that due to the very low abundance of ^{15}N, the N isotope patterns could only be observed for a few nitrided products; despite that, the consistency of the N isotope patterns for the nitrided products has strongly supported the reliability of the identification results.

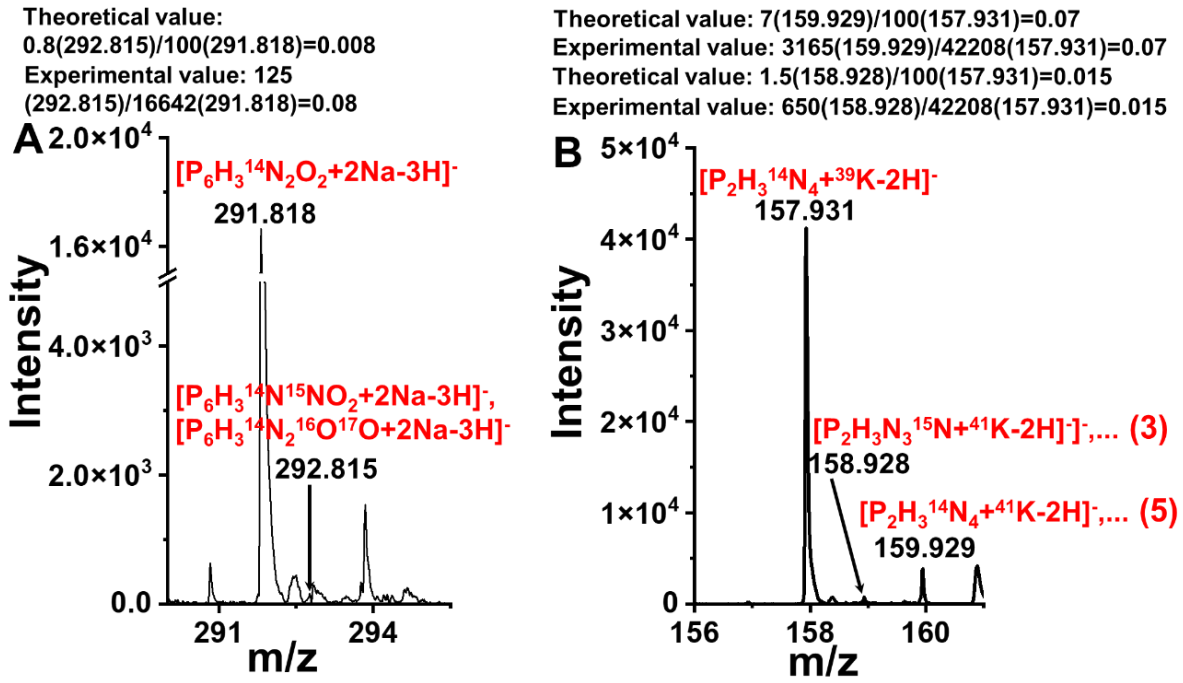

Figure S11. The stable isotope patterns verifying the hydrogen-to-metal exchange mechanism in negative-ion LDI-TOF MS. The left and right column show the peaks of two nitrided products ([$P_6H_3N_2O_2$+2Na-3H] and [$P_2H_3N_4$+K-2H]) in LDI-TOF MS. N has two natural stable isotopes (^{14}N and ^{15}N) with the abundance ratio of 99.634%:0.366%. K has three natural stable isotopes (^{39}K, ^{40}K, and ^{41}K) with the abundance ratio of 93.3%: 0.0117%:6.7%. The theoretical value of the K, N, and O isotope patterns for the nitrided products was calculated by the Compass IsotopePattern Software (Bruker). It can be seen that the N, O and K isotope patterns could be observed for the identified nitrided products ([$P_6H_3N_2O_2$+2Na-3H]$^-$ and [$P_2H_3N_4$+K-2H]$^-$), and the experimental values of the K, N, and O isotope patterns for the nitrided products were highly consistent with the theoretical values, indicating that the identified products through hydrogen-to-metal exchange mechanism were accurate.

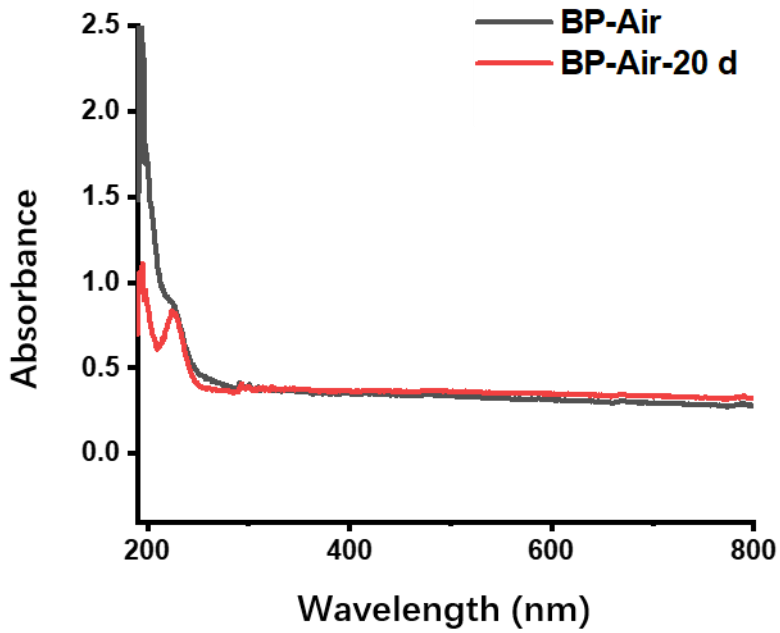

155

156 **Figure S12. UV-vis absorption of BP in air over time.** The spectra exhibited the absorption
157 of BP at 355 nm (the wavelength used in the LDI process). After degradation for 20 d, the
158 absorption of BP showed some redshift probably due to the generation of some chromophores
159 (i.e., -P=O-).

160

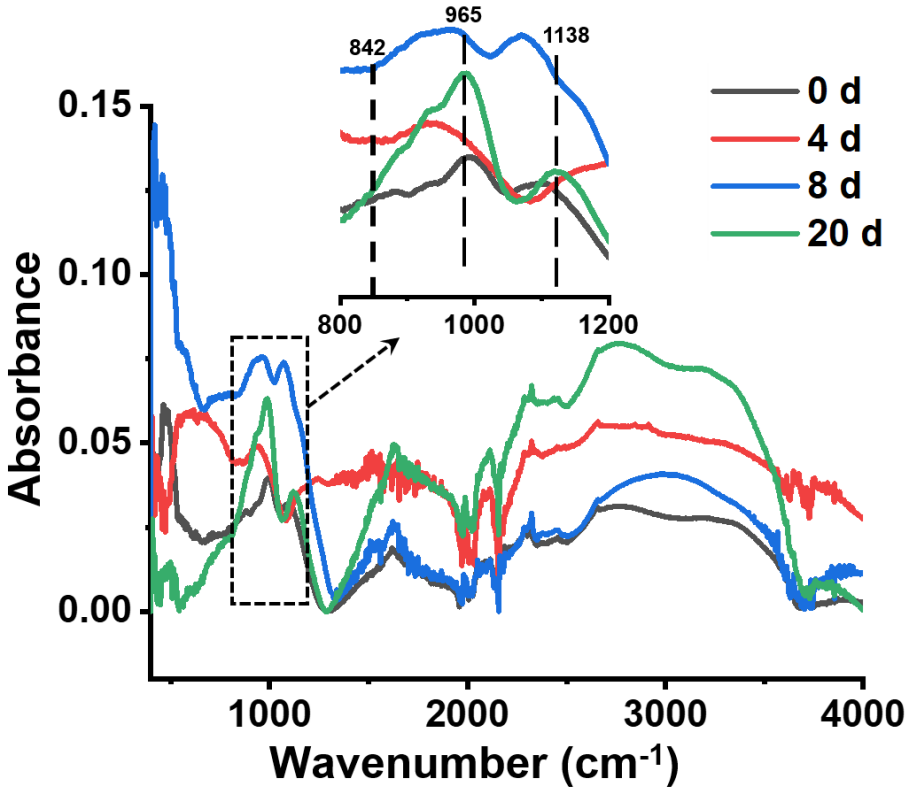

Figure S13. FT-IR characterization of BP in air over time. The 800 to 1200 cm^{-1} region is enlarged in the inset. The material exhibited absorption peaks at 1138 and 965 cm^{-1}, which are assigned to the -P=N- stretching vibration and the feature absorption of -P–O–P- stretch, respectively. It can be observed that with the degradation processing, the oxygen/nitrogen-containing functionalities showed a gradual increasing and then decreasing trend, corresponding to the generation of O and N-containing intermediates and their further degradation process.

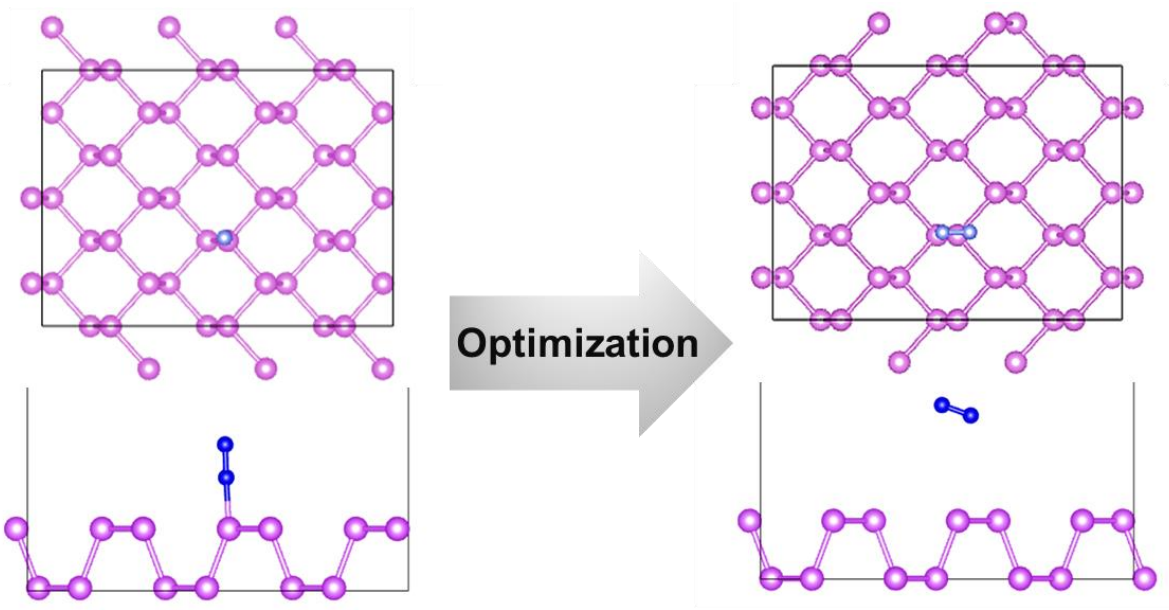

Figure S14. DFT and molecular dynamics computations of the chemisorption of N_2 on BP in the ambient environment. Atomic structures of N_2 on pristine monolayer (1L) BP are shown, and N_2 is individually adsorbed on the surface of 1L BP. N_2 interacts with the surface of BP with an energy decrease of 0.33 eV, indicating that the chemisorption of N_2 on BP reduces the energy barrier for the oxidation of BP and makes it relatively stable. The detailed parameters of DFT molecular dynamic model are listed in **Table S8**.

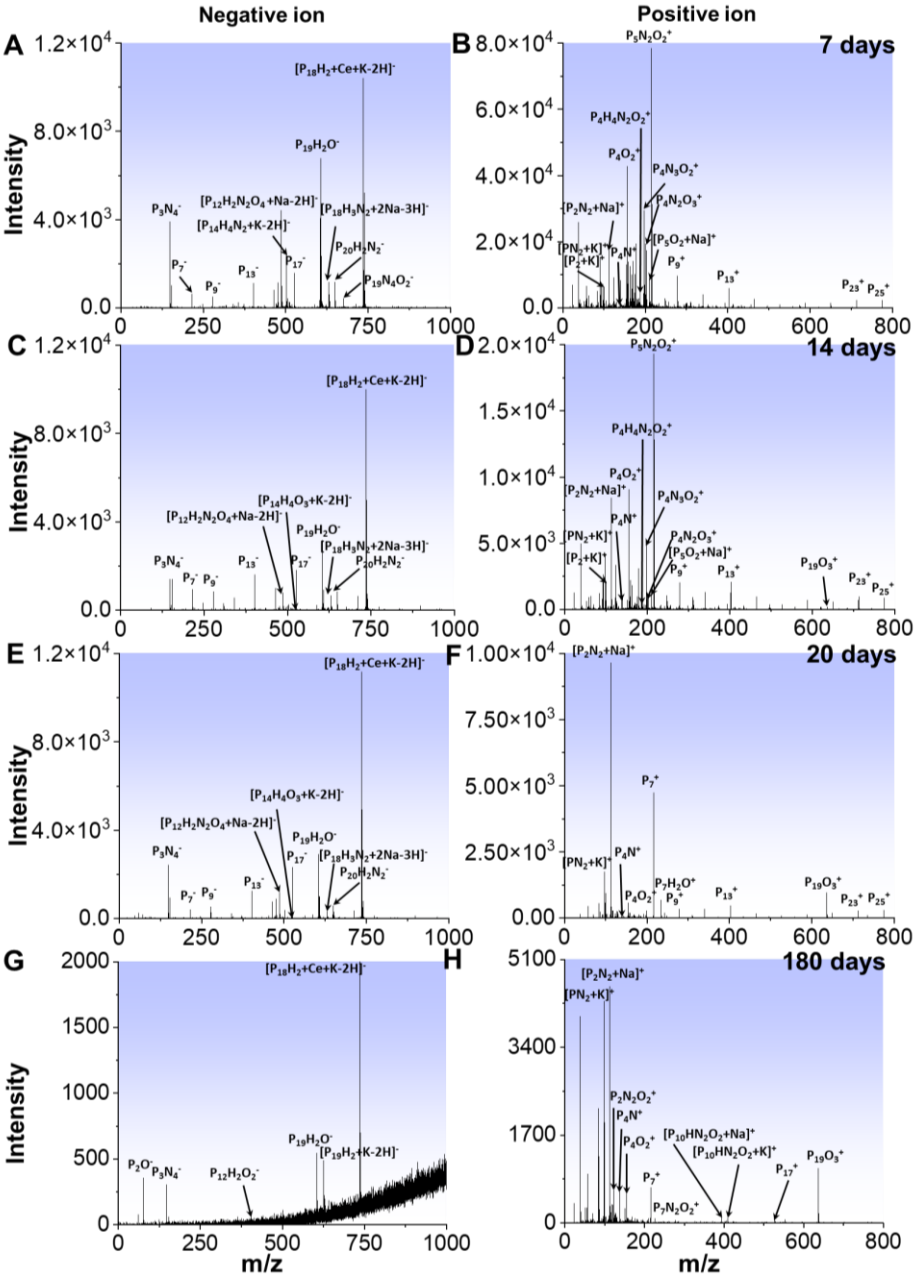

Figure S15. Monitoring the ambient stability of untreated CeBP by LDI-TOF MS. (**A, B**) 7 days, (**C, D**) 14 days, (**E, F**) 20 days, and (**G, H**) 180 days. The left and right columns represent the spectra obtained in the negative and positive ion mode, respectively. A variety of peaks of oxidized and nitrided products were yielded in the spectra with the peak intensities varying with the degradation time. For each spectrum, 20 shots were made in different sample regions and the spectrum with average intensities is shown to ensure the representativeness.

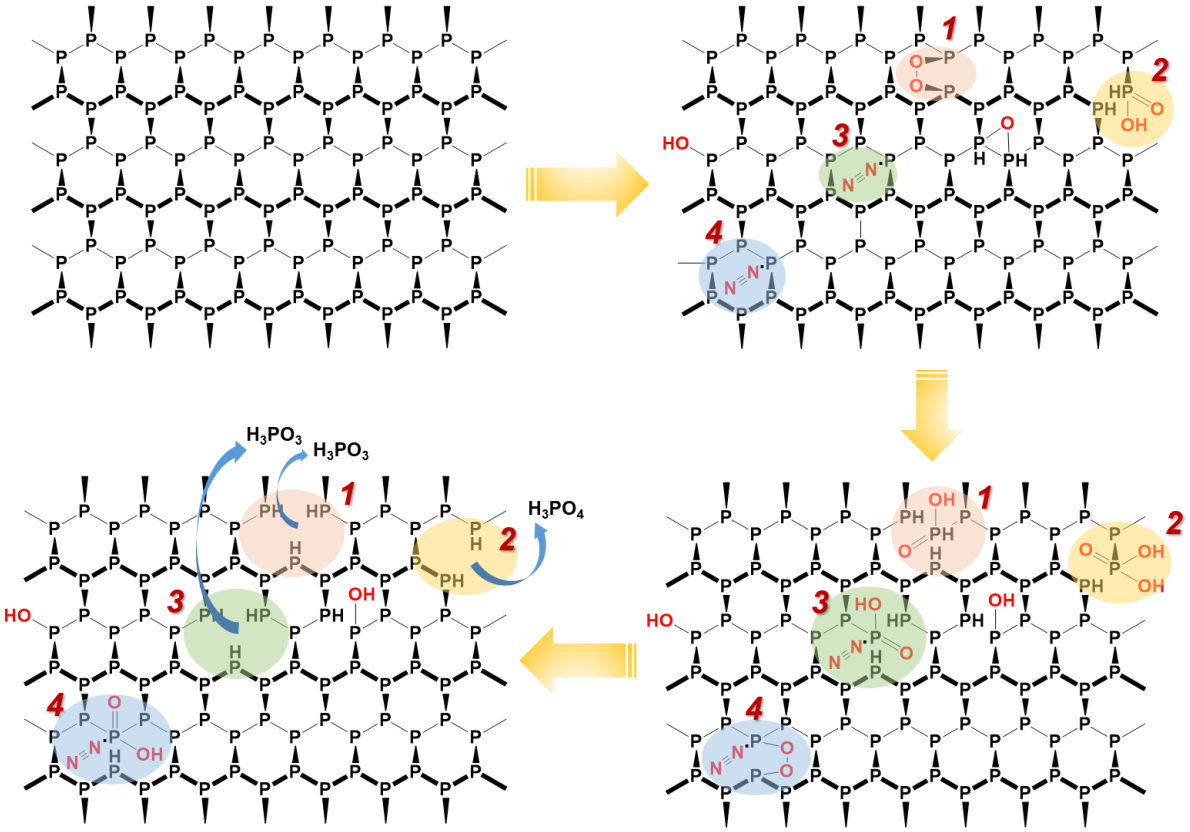

Figure S16. Possible degradation pathways of CeBP in the ambient environment based on LDI-MS fingerprinting results. The colored shadows indicate different possible degradation pathways (**1-2**: oxidation route; **3-4**: N_2-addition oxidation route). *Note:* this figure only shows the pathways and intermediates derived from the MS fingerprints and may not include all possible degradation pathways. Compared with BP, CeBP was more stable due to the presence of Ce coating. From the LDI-MS fingerprinting, the proportion of N_2-addition oxidation to direct oxidation in CeBP was higher than BP.

References for SI

1. Ahmed, T.; Balendhran, S.; Karim, M. N.; Mayes, E. L. H.; Field, M. R.; Ramanathan, R.; Singh, M.; Bansal, V.; Sriram, S.; Bhaskaran, M.; Walia, S., *npj 2D Mater. Appl.,* **2017,** *1*, 18.